

Article

Calculation of Column Pile Heave in Deep Excavation Based on the Rebound–Recompression Method

Kaiwen Yang ¹, Yun Chen ² and Zhuofeng Li ^{3,*}

¹ MOE Key Laboratory of Soft Soils and Geoenvironmental Engineering, Zhejiang University, Hangzhou 310058, China; 12012001@zju.edu.cn

² Center for Balance Architecture, The Architecture Design and Research Institute of Zhejiang University, Hangzhou 310013, China; hoppercy@sohu.com

³ School of Civil Engineering and Architecture, Guangxi University, Nanning 530004, China

* Correspondence: lizhfg@126.com

Abstract: Excessive column pile heave may result in engineering disasters such as instability of retaining structures and cracking of existing engineering piles in deep excavations. However, factors such as support weight, changeable support restraint resistance, and soil disturbance at the bottom of the excavation are often ignored or simplified in existing calculation methods but have a significant impact on the calculation results. Based on field soil parameters obtained by the rebound–recompression method, a semi-analytical method is proposed for estimating column pile heaves in a deep excavation. This method considers the influence of soil disturbance, the weight of the retaining structure, and the changeable horizontal support restraint, making the calculation result more consistent with the realistic situation. This method can also be used to analyze load transfer between the pile and the surrounding soil. The rationality of this proposed calculation method is verified by measured data, where the variation in pile stress state during deep excavation is analyzed. Finally, a parametric study is conducted, and the results show that the excavation size and the excavation depth have a great influence. However, the heave is hardly affected by the value of the limit relative displacement. The use of long piles with small diameter and the method of small block excavation are effective means to control the column pile heave. When the excavation area is large or the effective pile length is short, the factor of the position of the column pile cannot be ignored.

Keywords: deep excavation; column pile; Mindlin stress solution; soil disturbance; field compression curve



Citation: Yang, K.; Chen, Y.; Li, Z. Calculation of Column Pile Heave in Deep Excavation Based on the Rebound–Recompression Method. *Buildings* **2024**, *14*, 1477. <https://doi.org/10.3390/buildings14051477>

Academic Editors: Eugeniusz Koda and Bingxiang Yuan

Received: 29 March 2024

Revised: 3 May 2024

Accepted: 15 May 2024

Published: 18 May 2024



Copyright: © 2024 by the authors. Licensee MDPI, Basel, Switzerland. This article is an open access article distributed under the terms and conditions of the Creative Commons Attribution (CC BY) license (<https://creativecommons.org/licenses/by/4.0/>).

1. Introduction

In recent years, the increased demand for extensive underground space utilization has led to larger-scale deep excavations. Excavation is a process of gradual stress release that results in soil rebound deformation and engineering pile heave. Heave-induced tension may occur in these installed piles, where upward movement is ongoing near the top of the pile, while the smaller deformation of the soil near the lower end of the pile acts as a disincentive to pile displacement. Cracking of the concrete will occur consequently if there is insufficient tensile reinforcement and it is under a large pile tension [1–3]. The column pile, composed of an upper steel column and a lower load-bearing pile, is the vertical support system of the retaining structure. Large column pile heave will cause internal force redistribution in the retaining structure, which affects the stability of the retaining structure and its support system [4–6]. Especially for soft soil areas, the poor soil properties make engineering more challenging [7,8]. In current projects, little attention is paid to column pile heave, though more and more projects have begun to monitor it [9–12]; typically, only a simple estimation is made for this problem at the design stage for the retaining structure. So, a more precise calculation method for predicting the column pile heave is necessary.

Improved methods can provide the theoretical basis for protecting the engineering piles and improving the retaining structure's stability.

Many factors affect the column pile heave: the excavation size, form and size of the retaining structure, soil quality, soil stress history, construction method, and so on [13–17]. A number of researchers have analyzed the influence of soil rebound on piles by assuming that the soil rebound distribution was regularly distributed along the depth direction based on the elastic theory method. Zheng et al. [18] carried out a series of statistical analyses and research on the column pile heave of a deep excavation in the Tianjin metro and summarized their proposed laws about this engineering problem and influencing factors. Yang and Lu [19] proposed a method for calculating the heave and force of a vertical column pile based on the coordination of pile-soil displacement and the load balance, but the method assumes that the pile is rigid and does not consider the influence of rebound depth, so it cannot describe the actual situation accurately and has some limitations. He [20] put forward the calculation method based on the Mindlin stress solution, and the influence depth of rebound was determined by finite-element simulation. In that method, the relationship between column pile length and rebound depth was studied, but the deformation coordination of pile and soil was not clear, and the support weight was neglected. Based on the generalized load transfer method and the calculation method of soil rebound deformation distribution at the base, Lou et al. [21] put forward a calculation method, and factors such as pile diameter, step-by-step excavation, and the impact of struts were considered. Zhai et al. [22] put forward a simplified calculation method of column pile heave under different excavation conditions and considered the influence of superstructure stiffness according to typical cases.

In practice, only with difficulty can soil deformation be described by a single modulus; further, soil properties are highly regional, so special laboratory tests are always required to determine the parameters. In obtaining the soil sample and preparing it for the laboratory test, soil stress release and disturbance occur simultaneously, resulting in differences between the laboratory compression curves and field compression curves [9,23–25]. To overcome this problem, Li et al. [26] proposed a modified approach, the rebound–recompression method (RRM), to obtain the field rebound–recompression curve that can reflect the actual situation more accurately.

Based on the RRM [26] and the Mindlin stress solution [27], a semi-analytical method for calculating the column pile heave in deep excavation is proposed in this paper. The conditions of pile-soil deformation coordination and force equilibrium are obtained by iterative calculation. The proposed method can consider factors such as support weight, support restraint, variable cross-section of pile body, and excavation size and shape. These factors have not been paid attention to in the previous methods but have an impact on the heave prediction that cannot be ignored. In addition, load transfer characteristics between piles and soil can also be analyzed. This method was verified by the measured data of the Centrifugal Hyper-gravity and Interdisciplinary Experiment Facility (CHIEF) project, one of the Major National Science and Technology Infrastructure Projects in China. The interaction between soil and pile and the pile stress state were also analyzed in this case. Finally, a parametric study was conducted to investigate the effects of excavation and soil properties on the column pile heave.

2. Methods

2.1. Calculation of Soil Rebound Based on the RRM

The Mindlin stress solution and the RRM are used to calculate the rebound deformation of the bottom soil caused by excavation. In 1936, Mindlin [27] gave the solution of stress and displacement generated at any point by a vertical concentrated force acting on the interior of a semi-infinite elastic body. Compared to the Boussinesq solution, the Mindlin stress solution breaks through the limits of the forces acting on the soil surface. In addition, the soil rebound calculation method based on the Mindlin stress solution can consider the influence of the excavation shape and spatial effect, so it is widely used in

excavation engineering. Li et al. [26] proposed the RRM, which seeks to obtain the in situ soil parameters for field rebound–recompression curves. The use of the RRM enables the utilization of in situ soil parameters for the calculation of soil rebound resulting from excavation, resulting in more realistic outcomes relative to those generated by laboratory-disturbed soil parameters. In the calculation method proposed in this study, the Mindlin stress solution is used to calculate the changes in soil stress caused by excavation, and the RRM is used to correct soil parameters.

2.1.1. Unloading Stress Caused by Excavation

A concentrated load Q is applied at a depth h from the ground surface in the soil, and the vertical additional stress at any point M in the soil is

$$\sigma_z = \frac{Q}{8\pi(1-\mu)} \left[\frac{(1-2\mu)(z-h)}{R_1^3} - \frac{(1-2\mu)(z-h)}{R_2^3} + \frac{3(z-h)^3}{R_1^5} + \frac{3(3-4\mu)z(z+h)^2 - 3h(2+h)(5z-h)}{R_2^5} + \frac{30hz(z+h)^3}{R_2^7} \right] \quad (1)$$

where μ is Poisson's ratio, $R_1^2 = \rho^2 + (z-h)^2$, $R_2^2 = \rho^2 + (z+h)^2$, ρ is the horizontal distance between calculation point M and force Q , and z is the depth of calculation point M .

In the process of excavation, the stress of the soil is gradually released due to the weight of soil removed from the pit. Thus, the excavation unloading can be simulated by applying a uniformly distributed vertical load at the bottom of the excavation, which is equal to the weight of the excavated soil. The vertical stress at any point in the soil below the pit bottom can be obtained by the surface integral of the uniform vertical distribution load on the horizontal plane according to Equation (1), which is the unloading stress caused by soil excavation (Figure 1). It has been widely recognized as correct and has been applied to calculate the soil rebound deformation caused by excavation, based on the Mindlin stress solution [20,28–30]. The calculation depth can be determined based on the condition that the additional stress value is less than 0.2 times the self-weight soil stress value.

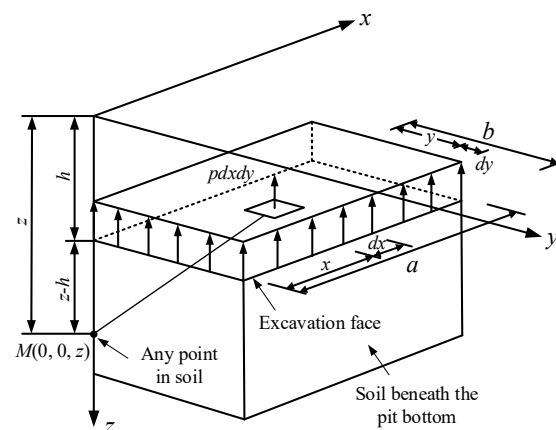


Figure 1. Calculation model of unloading stress under deep excavation.

2.1.2. Calculation of the In Situ Void Ratio and Field Recompression Index

The compression curve (e - $\log p$ curve, which describes the relationship between the void ratio and logarithmic pressure), reflecting soil consolidation characteristics, under a logarithmic coordinate system, can be obtained by laboratory tests. According to this curve, two parameters for calculating soil deformation can be obtained: the rebound index (C_{LR}) and the initial void ratio (e_0). These two parameters are the key to calculating soil deformation accurately. However, the process of sampling and sample preparation (e.g., drilling, sample transportation, storage, sample cutting, installation, and other processes) inevitably disturbs the sample, especially those soft soils with highly sensitive; hence, the compression curve obtained by laboratory test results does not reflect the actual properties

of the soil in the field, making the final calculation results uncertain. According to the literature proposing the RRM [26], the rebound curve obtained from the laboratory test is modified, and the field recompression index (C_{FR}) and in situ initial void ratio (e_{v0}) are obtained.

The relationship between the in situ rebound–recompression curve modified by the RRM and the laboratory compression curve [26] is shown in Figure 2; the method of obtaining parameters C_{FR} and e_{v0} can also refer to this figure. Point A represents that the soil sample is under the in situ stress state, and after soil sampling and sample preparation, the soil is unloaded to point B. Point C is the state when the soil sample is reloaded in the laboratory to the same stress values that existed in situ. These two processes constitute the first unloading–reloading cycle ($A \rightarrow B \rightarrow C$), and another unloading and reloading cycle should be applied at the end of the first reloading ($C \rightarrow D \rightarrow E$) to obtain the laboratory recompression index. We assume that there is only elastic strain produced in the process of soil rebound deformation under unloading and ignore the additional plastic strains during the first reloading cycle. These are commonly used assumptions in previous related research, and they have almost no impact on the final calculation results. The difference in the void ratio between points A and C, Δe_d , is the decrease in the void ratio caused by soil disturbance during sampling and sample preparation, which is equivalent to the difference in the void ratio between point B and point D. Point P is the undisturbed state of the soil sample under unloading with a void equal to the void ratio of point B plus Δe_d . Point Q is the in situ state of the soil under the pre-consolidation pressure or the structural yield stress σ'_y . Finally, using knowledge of the characteristics of the soil e - $\log p$ curve, the laboratory compression curve is extended until it intersects the $0.42e_0$ line at point I (the critical state point at which most natural soil curves tend to converge), and point Q is connected with point I. The curve PQI is the curve after being modified by the RRM, considering the soil disturbance.

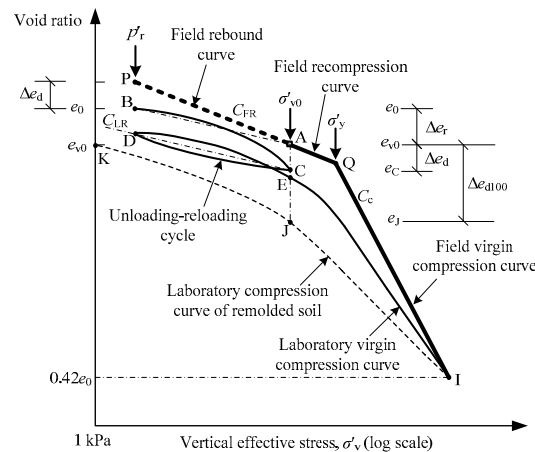


Figure 2. Method of estimating the field rebound–recompression curve based on the RRM.

According to the method described above, e_{v0} can be obtained by drawing a line with the same slope as the second unloading–reloading cycle and passing through point B and intersecting the straight σ'_{v0} line at point A. C_{FR} can be obtained from the slope of the line AP. The field recompression index (C_{FR}) and the in situ initial void ratio (e_{v0}) can be calculated by the following formulas:

$$e_{v0} = e_0 - C_{LR} \log \frac{\sigma'_{v0}}{p'_r} \quad (2)$$

$$C_{FR} = C_{LR} + \frac{\Delta e_d}{\log \frac{\sigma'_{v0}}{p'_r}} \quad (3)$$

where e_{v0} is the in situ initial void ratio, e_0 is the initial void ratio, C_{FR} is the field recompression index, C_{LR} is the recompression index, Δe_d is the decrease in the void ratio caused by soil disturbance during sampling and sample preparation, and p'_r is the residual effective stress, which can be measured by a test or estimated according to the empirical method.

2.1.3. Calculation of Soil Rebound Deformation

After calculating the unloading stress, in situ void ratio, and field recompression index, the layer-wise summation method is adopted according to the traditional foundation settlement calculation method, which is calculated as follows:

$$S_s = \sum_{i=1}^n \frac{C_{FR_i}}{1 + e_{v0_i}} H_i \log \frac{\sigma'_{v0_i} - \Delta\sigma_{z_i}}{\sigma'_{v0_i}} \quad (4)$$

where S_s is the final soil rebound deformation, C_{FR_i} is the field recompression index of the i -th layer of soil, e_{v0_i} is the in situ void ratio of the i -th layer of soil, H_i is the thickness of the i -th layer of soil, σ'_{v0_i} is the vertical effective stress of the i -th layer of soil before the excavation, and $\Delta\sigma_{z_i}$ is the additional vertical effective stress of the i -th layer of soil.

For soils of better properties, such as sand or bedrock, where the disturbance has less impact, the unloading modulus of the soil can also be used to calculate soil rebound deformation by the following equation:

$$S_s = \sum_{i=1}^n \frac{\Delta\sigma_{z_i}}{E_{t_i}} H_i \quad (5)$$

where E_{t_s} is the unloading modulus of the i -th layer of soil.

2.2. Calculation of Column Pile Heave

2.2.1. Analysis of Force and Rebound Deformation

The force and deformation of the column pile are more complex than those of the traditional compression and uplift piles subjected to only a single directional load. The distributions of pile axial force and pile-side frictional resistance are difficult to determine directly because of the upward deformation of the column pile under the action of soil rebound on the side of the pile and the load caused by support weight and restraint. The existence of pile foundations at the bottom of the excavation face inhibits the rebound deformation of the soil, so the actual rebound deformation is smaller than the free rebound deformation. There is a neutral point at a certain depth below the excavation surface, where the displacement of the pile is equal to that of the soil, so the frictional resistance there is zero. There are two conditions: (a) Above the neutral point, the soil moves upward relative to the pile, due to the large soil rebound deformation. The pile body is subjected to the vertical upward friction exerted by the soil, and the soil around the pile is also subjected to the vertical downward reaction from the pile. (b) Below the neutral point, the soil moves downward relative to the pile with a small soil rebound deformation. The pile body is subjected to the vertical downward friction exerted by the soil, and the soil around the pile is also subjected to the vertical upward reaction from the pile. The simplified pile-soil force diagram is shown in Figure 3.

In addition to bearing the frictional resistance of the pile-side soil, the column pile also bears the load of the retaining structure, including the weight of the structure and the reaction force of the horizontal support restraint. This kind of load acts on the column vertically and to a certain extent restrains the rebound of the column pile. When the pile is subjected to small vertical upward friction caused by soil rebound but with a large vertical downward load, the load of the retaining structure may be greater than the maximum friction that the soil can provide, at which time the column pile appears to settle.

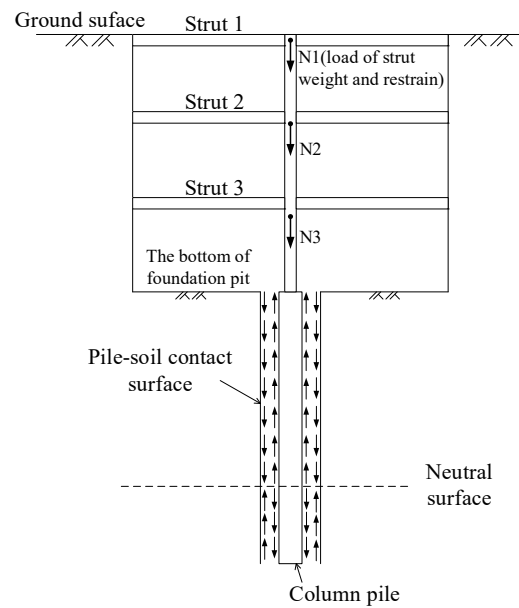


Figure 3. Simplified diagram of forces acting on a column pile in deep excavation during unloading.

When the excavation is deep and the length of the pile is short, the rebound deformation of the soil below the end of the pile cannot be neglected. Since this part of the soil is below the pile end, the column pile is mainly affected by the frictional resistance on the side of the pile. Therefore, when calculating the rebound of the soil below the end of the pile, the impact of the column pile can be ignored. Assuming that this part of the soil produces a free rebound field, it can be calculated according to the soil rebound calculation method described Section 2.1.3. The final rebound displacement at the top of the column pile can be expressed as

$$S = S_p + S_{s1} \quad (6)$$

where S_p is the pile top rebound displacement caused by the soil rebound deformation within the pile length, and S_{s1} is the rebound deformation of the soil below the pile end.

2.2.2. Pile-Side Friction and Force Balance

The load transfer between the pile and the soil by frictional resistance is related to the pile-soil relative displacement, which is the key to realizing pile-soil deformation coordination. It is assumed that the relationship between the frictional resistance and the relative displacement conform to the ideal elastoplastic model [19], as shown in Figure 4. When the relative displacement is small, the frictional resistance increases linearly with the relative displacement; when the relative displacement exceeds the limit of the linear displacement/resistance relation, the frictional resistance no longer increases with the relative displacement. The frictional resistance can be calculated according to the following formula:

$$\tau = \begin{cases} \frac{\tau_{max}}{u_{max}} \cdot u, & u < u_{max} \\ \tau_{max}, & u \geq u_{max} \end{cases} \quad (7)$$

where τ is the pile-side frictional resistance, u is the relative displacement between the soil and the pile, τ_{max} is the ultimate value of the pile-side frictional resistance, and u_{max} is the limit of the relative displacement.

The ultimate value of the pile-side frictional resistance τ_{max} can be calculated by the following equation:

$$\tau_{max} = \begin{cases} \zeta \sigma', \zeta \sigma' \leq f_s \\ f_s, \zeta \sigma' > f_s \end{cases} \quad (8)$$

where ζ is the pile-side frictional resistance coefficient, σ' is the vertical effective stress on the side of the pile, and f_s is the ultimate frictional resistance of the soil.

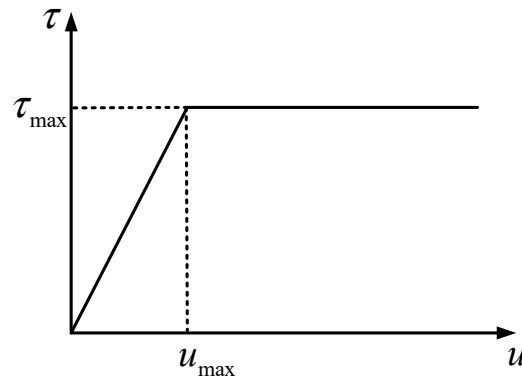


Figure 4. Model of soil resistance along the pile.

Column pile heave occurs under the combined action of pile-side friction resistance and retaining structure load. After the column pile heave is stable, the pile is in a state of force equilibrium, i.e.,

$$\sum_{i=1}^{n_1} \tau_i h_i \pi d + \sum_{i=1}^{n_2} F_i + \sum_{i=1}^{n_2} k_i S_{strut_i} = 0 \quad (9)$$

where n_1 is the total number of layers after discretization of the column pile, n_2 is the number of horizontal support layers, τ_i is the frictional resistance around the column pile at the i -th-layer depth, h_i is the thickness of the i -th layer, d is the pile diameter, F_i is the weight of the i -th-layer horizontal support acting on the column, k_i is the restraint stiffness of the i -th-layer horizontal support to the column pile, and S_{strut_i} is the rebound deformation at the i -th-layer horizontal support.

2.2.3. Calculation of Soil Rebound Considering the Action of Frictional Resistance

The column pile is subjected to frictional resistance from the soil, while the soil is subjected to the reaction force from the pile. The deformation of the soil caused by this force can be obtained by integrating the Mindlin stress solution, as shown in Figure 5.

The soil is discretized into n layers; each layer of soil is considered to be subjected to the frictional resistance from the pile acting uniformly on the pile-soil contact surface, and the magnitude of the frictional resistance in the same layer is certain and can be determined according to Section 2.2.3. The additional stress in the i -th layer of soil can be expressed as the sum of the effects of the frictional resistance on all the soil layers above the layer. The additional stress in soil generated by each layer's frictional resistance can be obtained by integrating the Mindlin stress solution over the pile-soil contact surface, and the final additional stress can be calculated by the following equation:

$$\Delta\sigma_{f_i} = \sum_{j=1}^i 2 \int_{z_j-h_j/2}^{z_j+h_j/2} \int_0^{\pi/2} \rho_i \tau_j \cos \theta d\theta dz \quad (10)$$

where $\Delta\sigma_{f_i}$ is the additional stress caused by the frictional resistance of the pile in the i -th layer of soil, τ_j is the frictional resistance at the pile-soil interface of the j -th layer, and ρ_i is the influence coefficient of a single vertically concentrated load in the i -th layer of soil, which can be calculated by the following equation:

$$\rho_i = \frac{(1+\mu)}{8\pi(1-\mu)} \left[\frac{3-4\mu}{R_1} + \frac{5-12\mu+8\mu^2}{R_2} + \frac{c_1^2}{R_1^3} + \frac{(3-4\mu)c_2^2-2zc_2+2z^2}{R_2^3} + \frac{6zc_2^2(c_2-z)}{R_2^5} \right] \quad (11)$$

where $c_1 = z_i - z$, $c_2 = z_i + z$, $R_1^2 = (d \cos \theta)^2 + z_1^2$, and $R_2^2 = (d \cos \theta)^2 + z_2^2$.

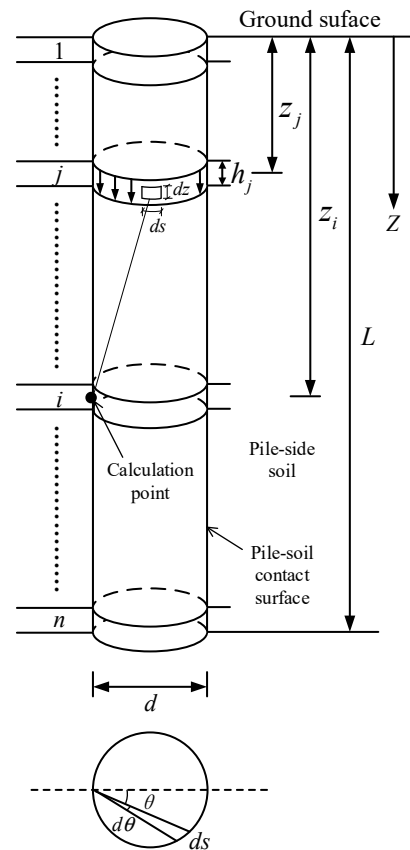


Figure 5. Sketch map of integral of soil stress under friction.

Thus, the pile-side soil rebound under the influence of the pile can be calculated by adding $\Delta\sigma_{f_i}$, the additional stress generated by the pile-side frictional resistance, to Equation (4), which can be modified as follows:

$$S_s = \sum_{i=1}^n \frac{C_{FR_i}}{1 + e_{v0_i}} H_i \log \frac{\sigma'_{v0_i} - (\Delta\sigma_{z_i} + \Delta\sigma_{f_i})}{\sigma'_{v0_i}} \quad (12)$$

And Equation (5) can be modified as follows:

$$S_s = \sum_{i=1}^n \frac{\Delta\sigma_{z_i} + \Delta\sigma_{f_i}}{E_{t_i}} H_i \quad (13)$$

It should be noted that of the positive and negative of $\Delta\sigma_{f_i}$, positive means the additional stress is in the same direction as the excavation unloading stress, vertically upward, while negative means the stress is in the opposite direction as the excavation unloading stress, vertically downward.

2.3. Calculation Steps and Iterative Solution

Using the above method, the column pile heave can be calculated by iterative calculations. The calculation steps and iterative solution process are as follows:

(a) Discretize the pile and the soil around the pile into several layers. According to the theory of soil rebound calculation based on the RRM, obtain the free rebound of soil under the non-pile condition after excavation and unloading. Record the soil rebound below the end of the pile as S_{s1} , and record the soil rebound within the range of pile length as S_{s2} .

(b) Determine the column pile subjected to frictional resistance according to the relative displacement of the pile and soil within the range of the pile length, combining with the

calculation model of pile-side frictional resistance. At the same time, the conditions of force balance must be met.

(c) Obtain the pile axial force by considering the column pile subjected to frictional resistance, load of horizontal support weight, and restraint. Calculate the pile deformation and the displacement of each of the pile's layers according to material mechanics. The displacement of the pile top is recorded as S_p .

(d) Recalculate the pile-soil relative displacement based on the pile deformation obtained in step (c), and calculate the reactive force on the soil from the pile. Then, calculate the additional stress caused by the frictional resistance in each layer of soil according to Equation (10), and recalculate the rebound deformation of the soil within the pile length and the displacement of each layer of soil according to Equation (12) or Equation (13).

(e) Repeat steps (b) to (d) several times, and when the relative error of the calculation results obtained over the last two cycles is small enough, consider the results to be converged, and record the S_p . The final column pile heave can be calculated according to Equation (6).

On this basis, the MATLAB calculation program is prepared, and the flowchart is shown in Figure 6.

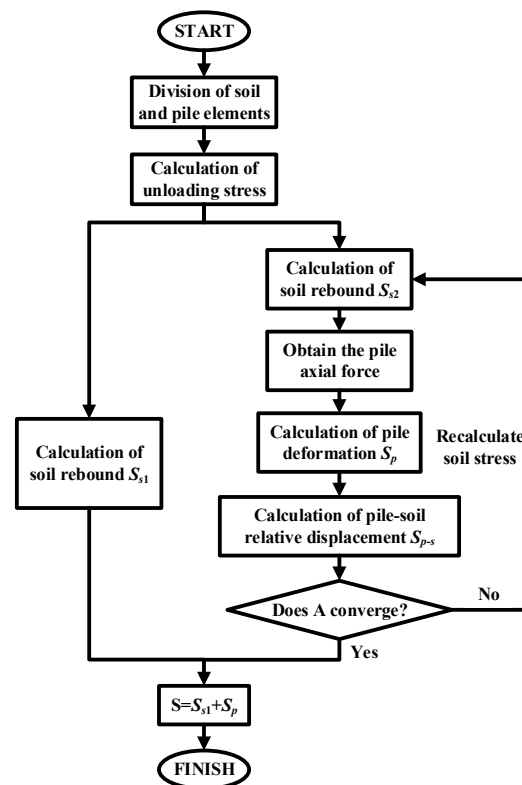


Figure 6. Flowchart of the calculation of column pile heave.

3. Results and Validation

The calculation method proposed in this paper is validated by an engineering example, and the stress state of the column pile in this case at different excavation stages is also analyzed by this method.

3.1. Project Overview

The Centrifugal Hyper-gravity and Interdisciplinary Experiment Facility (CHIEF) is one of the constructs of the Major National Science and Technology Infrastructure Projects in Hangzhou, Zhejiang Province, China. Due to the large excavation depth of the foundation for the CHIEF mainframe equipment and the stringent construction standards as a foundation for substantial power equipment, detailed monitoring was carried out during

excavation. Seven monitoring points, labeled S1 through S7, were arranged to record the column pile heave at the completion of each stage of excavation. The layout of the excavation and the column pile heave monitoring points are shown in Figure 7. The column pile heave was obtained through three-dimensional coordinate measurement using a total station. The excavation area was rectangular, with a width of 27 m and a length of 101 m. From north to south, the excavation area comprised three areas: a high-speed machine pit area, a heavy-duty machine pit area, and a model machine pit area. The high-speed machine pit area was the deep excavation area, with an excavation depth of 38.3 m; it was retained by a 46 m deep and 1.2 m thick cast-in-place diaphragm wall with eight levels of in situ concrete struts; the heavy-duty machine pit area and the model machine pit area were the shallow excavation areas, with an excavation depth of 23.95 m; these were retained by a 40 m deep and 1 m thick cast-in-place diaphragm wall with five levels of in situ concrete struts. The column pile heave monitoring points S1 through S5 were located in the shallow excavation area, and the piles were placed using the cast-in situ bored piles with a diameter of 800 mm and a length of 38.95 m. The monitoring points S6 and S7 were located in the deep excavation area, and the piles were cast-in situ bored piles with a diameter of 800 mm and a length of 48.3 m. The section of retaining structures is shown in Figure 8.

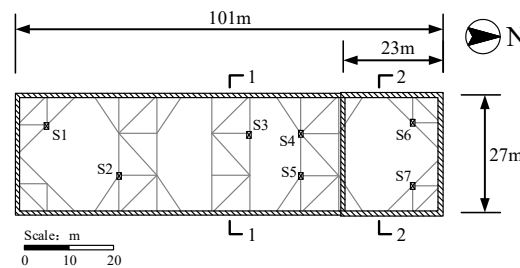


Figure 7. Excavation plan and arrangement of the monitoring points.

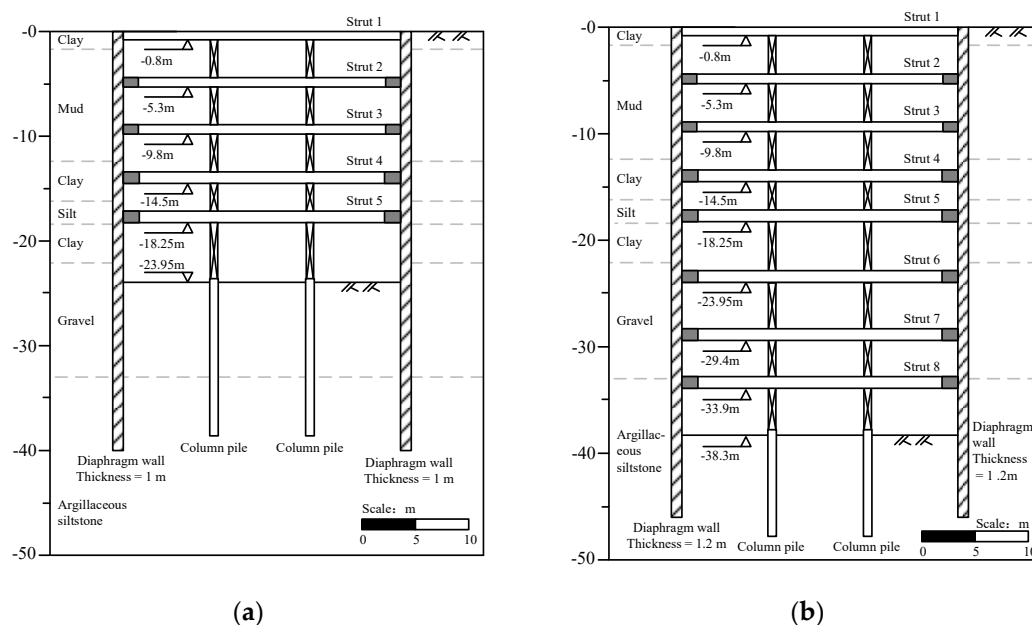


Figure 8. Section of retaining structures: (a) Section 1-1 (shallow excavation area); (b) Section 2-2 (deep excavation area).

3.2. Site and Geology

According to the detailed geological prospecting, combining the results of in situ and laboratory tests, the distribution of the site's soil layers and its basic physical and mechanical parameters are shown in Table 1. The moisture content was measured by the

oven-drying method, the unloading modulus was measured by indoor triaxial testing, the ultimate frictional resistance was estimated based on indoor triaxial testing combined with experience, and the limit of the relative displacement equals 2 mm in this case. The site was originally farmland and can be considered a greenfield site. The horizontal stratification of the soil was continuous, and the water table was generally flush with the surface.

Table 1. Physical and mechanical parameters of soils.

Soil Layers	Bottom Elevation/m	Water Content/%	Total Bulk Weight of Soil/ $\text{kN}\cdot\text{m}^{-3}$	Unloading Modulus/MPa	Ultimate Frictional Resistance of the Soil/kPa
① Silty clay	1.9	32.9	18.5	16.1	20 *
② Mud	12.6	53.5	16.5	15.0	18 *
③ Clay	13.8	37.7	17.8	15.1	20 *
④ ₁ Silty clay	15.1	25.7	19.5	23.5	30 *
④ ₂ Sandy silty clay	16.3	23.3	19.6	22.0	35 *
④ ₃ Silt	18.6	22.1	19.8	44.9	45 *
⑤ ₁ Clay	20.0	29.0	19.0	23.2	40 *
⑤ ₂ Silty clay	23.8	25.9	19.5	22.1	45 *
⑥ Gravel	32.6		24.0 *	75 *	75 *
⑩ ₁ Fully weathered argillaceous siltstone	34.6		20.0 *	70 *	70 *
⑩ ₂ Strong-weathered argillaceous siltstone	35.8		22.0 *	80 *	80 *
⑩ ₃ Middle-weathered argillaceous siltstone			25.0 *	200 *	85 *

Note: * indicates that the value was estimated empirically.

3.3. Measured and Calculated Results of Column Pile Heave

The field recompression index (C_{FR}) and in situ initial void ratio (e_{v0}) were first calculated according to the RRM, and the calculated results are shown in Table 2. For the soil layers that were more affected by disturbance (layer ②, ③, ④₁, ⑤₁, and ⑤₂), C_{FR} and e_{v0} were used to calculate according to Equation (12), while for the other soil layers, the unloading modulus given in Table 1 was used according to Equation (13). According to the size of the horizontal concrete support, the load of the support weight and restraint could be determined, in which the support weight load was always vertically downwards, and the direction of the restraint load was opposite to the deformation direction of its position. The specific values are shown in Table 3.

Table 2. The soil parameters after revision by the RRM.

Soil Layers	e_0	e_{v0}	C_{LR}	C_{FR}
② Mud	1.674	1.643	0.043	0.054
③ Clay	1.105	1.083	0.021	0.027
④ ₁ Silty clay	0.973	0.960	0.011	0.019
⑤ ₁ Clay	0.785	0.767	0.012	0.031
⑤ ₂ Silty clay	0.644	0.627	0.012	0.034

Note: e_{v0} and C_{FR} in the table are the values at the midpoint of each soil layer, which need to be calculated separately for each calculation layer after the soil has been discretized.

The measured results and calculation results of column pile heave according to the method in this paper are summarized in Table 4. The calculated results in this paper were in good agreement with the variation pattern of measured results, and their values were also very close. The column pile heave increased with the depth of excavation, and finally reached about 9 mm. The heave results showed a certain space effect, and the heave decreased with the increase in distance from the center of the excavation. This phenomenon has also been confirmed in the literature [31,32]. The calculated results in the case of without considering the support restraint are also summarized in Table 4 for comparison.

Table 3. Load of horizontal retaining structure weight and restraint.

Layer Number of Struts	Strut Size (Width × Height)/mm	Weight Load/kN	Restraint Load/kN·mm ⁻¹
Strut 1	800 × 900	100	10
Strut 2	1100 × 900	150	15
Strut 3	1100 × 900	150	15
Strut 4	1200 × 1100	200	25
Strut 5	1200 × 1100	200	25
Strut 6	1200 × 1100	200	25
Strut 7	1200 × 1100	200	25
Strut 8	1200 × 1100	200	25

Note: The load at the corner brace is appropriately discounted according to the values in the table.

Table 4. Measured and calculated value of column pile heave (unit: mm).

Excavation Depth		Measuring Point Number						
		S1	S2	S3	S4	S5	S6	S7
5.3 m	Measured result	1.62	1.13	1.52	0.91	0.60	0.47	0.73
	Considering support restraint	0.52	0.68	0.77	0.73	0.75	0.44	0.44
	Without considering support restraint	0.53	0.70	0.79	0.75	0.77	0.44	0.45
9.8 m	Measured result	1.81	1.79	2.90	1.99	2.62	2.05	2.73
	Considering support restraint	1.21	1.54	1.70	1.62	1.66	1.14	1.16
	Without considering support restraint	1.25	1.63	1.80	1.71	1.76	1.18	1.20
14.5 m	Measured result	3.18	3.12	4.42	4.83	4.24	4.90	4.97
	Considering support restraint	2.59	3.03	3.25	3.12	3.20	2.50	2.52
	Without considering support restraint	2.74	3.37	3.62	3.47	3.56	2.65	2.67
18.25 m	Measured result	5.69	5.29	5.74	5.98	5.61	5.53	5.45
	Considering support restraint	5.08	5.58	5.88	5.66	5.84	3.96	3.98
	Without considering support restraint	6.08	7.82	8.28	7.93	8.21	4.34	4.37
23.95 m	Measured result	6.71	6.67	7.29	7.51	7.65	6.97	6.80
	Considering support restraint	5.60	5.91	6.18	5.95	6.15	7.04	7.10
	Without considering support restraint	6.92	8.75	9.17	8.78	9.14	8.41	8.48
29.4 m	Measured result						7.22	7.12
	Considering support restraint						7.74	7.84
	Without considering support restraint						9.56	9.69
33.9 m	Measured result						8.50	8.53
	Considering support restraint						8.73	8.85
	Without considering support restraint						11.19	11.35
38.3 m	Measured result						8.94	9.03
	Considering support restraint						8.84	8.97
	Without considering support restraint						12.00	12.19

3.4. Analysis of the Results

The relationship curve between column pile heave (average value of each monitoring point) and excavation depth is shown in Figure 9; the figure shows there was a linear relationship between column pile heave and the excavation depth in this project, and the ratio of heave to excavation depth (S/H) was 0.0255% and 0.0248% in the measured and calculated results in this paper, respectively, which shows that the calculation method proposed in this paper is in good agreement with the measured results. According to the variation in the column pile heave and the excavation depth, the slope of S/H was steeper when the excavation depth was less than 25 m than it was with further excavation. This was related to the large vertical displacement of the horizontal support, which led to an increase in the restraint load and a reduction in the effective length of the pile subjected to frictional resistance. However, the S/H was 0.0322% when the support restraint was

not considered, about 30% larger than the measured results and the calculation results in this paper.

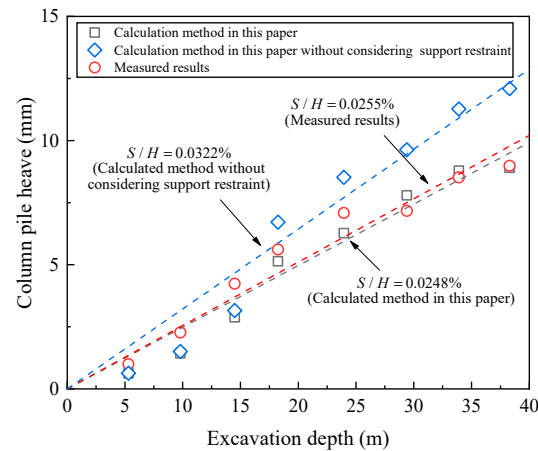


Figure 9. Comparison between calculated and measured value of upheave of column piles.

Based on the proposed method, the friction resistance on the side of the pile and the axial force of the pile were evaluated. Figure 10 shows the development curve of frictional resistance on the side of the pile (S5). With the excavation, column pile heave increased, pile-soil interaction became more obvious, and the friction resistance kept increasing. When the excavation depth is shallow, the upper part of the pile-side had obvious upward frictional resistance, while the lower part had an unobvious downward frictional resistance. When the excavation depth is deep, along the pile direction, the frictional resistance increased continuously to the limit value, after which it started to decrease, and the direction of frictional resistance reversed and developed to the reverse limit value. During excavation, the neutral point kept moving downwards, and when the excavation of the fifth layer was completed, the downward frictional resistance of the lower part of the pile had not reached the limit because the neutral point was already very close to the pile bottom.

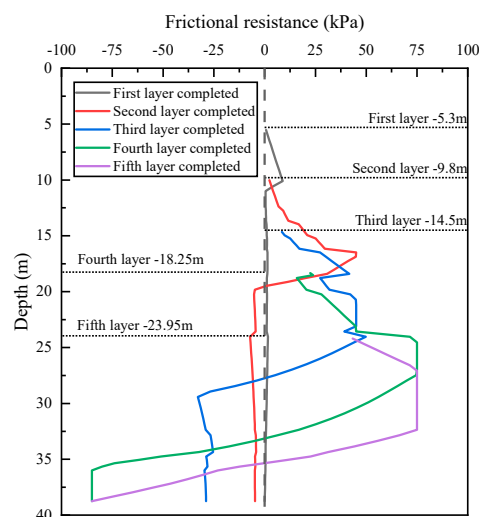


Figure 10. Variation in pile-side frictional resistance with excavation at the S5 measuring point.

Figure 11 exhibits the development curve of the pile axial force (S5), showing that the upper part of the pile was compressed by the support load, and the lower part of the pile was gradually transitioned to tensile stress under the action of frictional resistance on the side of the pile. The axial force at the end of the pile was close to 0, which was consistent with the conclusions in the literature [21]. With the increase in excavation depth, the maximum tension force on the pile increased first and then decreased. This was because the

soil rebound was relatively small when excavation depth was shallow, while the supporting load was larger and the pile length became shorter during deep excavation. The tensile force in the pile body would be smaller under the above factors, so the tension force on the pile reached the maximum at the completion of the fourth layer excavation, which was about 1100 kN. Under the same variation pattern of frictional resistance on the side of the pile, the maximum tension force position and the neutral point position of the pile kept moving down with the excavation.

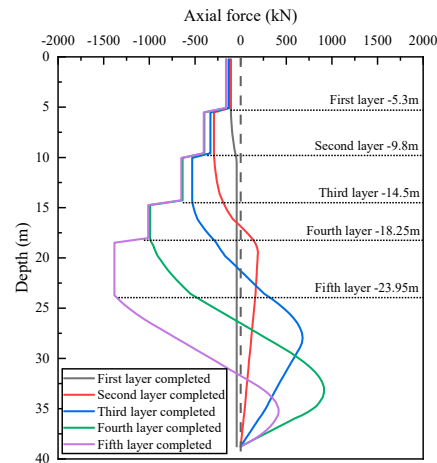


Figure 11. Variation in pile axial force with excavation at the S5 measuring point.

4. Discussion

A parametric study was conducted to investigate the effect of excavation size and the limit of the relative displacement u_{max} on the change in column pile heave. Figure 12 presents the calculation model. A square excavation area was adopted, and the excavation depth H_e was set as 20 m. The excavation width B and the effective pile length L_e were used as the variables in the parametric study. The pile diameter and the elastic modulus of the pile were set as 1 m/0.5 m and 30 GPa, respectively. The soil parameters adopted in the parametric study were same as the soil layer of silty clay (layer ④₁) and silt (layer ④₃) in the validation case, which had a unit weight of 20 kN/m³ and an ultimate pile-side frictional resistance value of 30 kPa. The support weight load and restraint load were 100 kN and 10 kN/mm to the first and second struts and were 150 kN and 15 kN/mm to the third and fourth struts. Table 5 shows the variables in the parametric study. The effects of excavation width B , effective pile length L_e , position of pile, and the limit of the relative displacement u_{max} were evaluated.

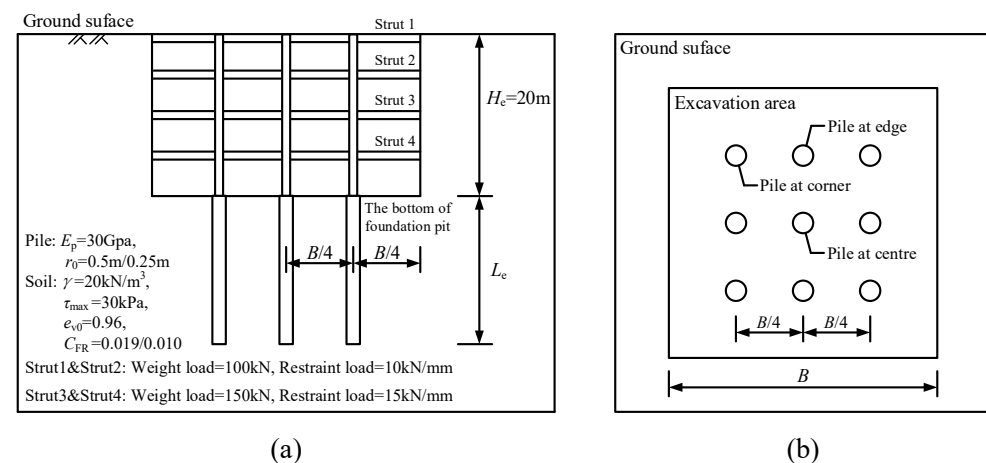


Figure 12. Calculation model for the parametric study: (a) profile of excavation; (b) plan of excavation.

Table 5. Variables in the parametric study.

L_e/H_e	0.5, 0.7, 0.8, 0.9, 1, 1.1, 1.2, 1.3, 1.4, 1.5
B/H_e	1, 1.5, 2, 2.5, 3, 3.5, 4, 4.5
u_{max}	2, 4, 6, 8, 10
Position of pile	Center, edge, corner

4.1. Effects of Effective Pile Length L_e

Figure 13 shows the relationship between column pile heave and effective pile length L_e . It can be seen in this figure that the column pile heave decreases nonlinearly with the effective pile length increase. When the ratio of the pile effective length to the excavation depth is greater than 1, i.e., pile effective length is greater than excavation depth, the heave decreases more rapidly. In the case of considering the support restraint, column pile heave is less affected by the change of effective pile length when L_e/H_e is within the range of 0.5–1. It is easy to understand that larger effective pile length, which means longer anchorage length, will cause smaller pile column heave. The smaller pile column heave leads to a smaller support constraint load. This can explain that effective pile length can more obviously affect column pile heave when L_e/H_e is within the range of 0.5–1 when not considering the constraint. The position of the pile can also affect the column pile heave. Smaller effective pile length and no consideration of support restraint will make its effect more obvious. Since silt is harder than silty clay, causing a smaller soil rebound deformation during excavation, the column piles in silt have smaller uplift compared to silty clay. However, the frictional force between the soil and the pile caused by the soil rebound deformation has been fully utilized in both types of soil, and the column pile heave in these two soils is very close. The diameter of the pile has a significant impact on the column pile heave. The contact area between the soil and small-diameter column piles is smaller with limited frictional force to drive the pile to heave, resulting in a smaller final column pile heave. Therefore, using longer piles with a small diameter can effectively control the column pile heave during excavation.

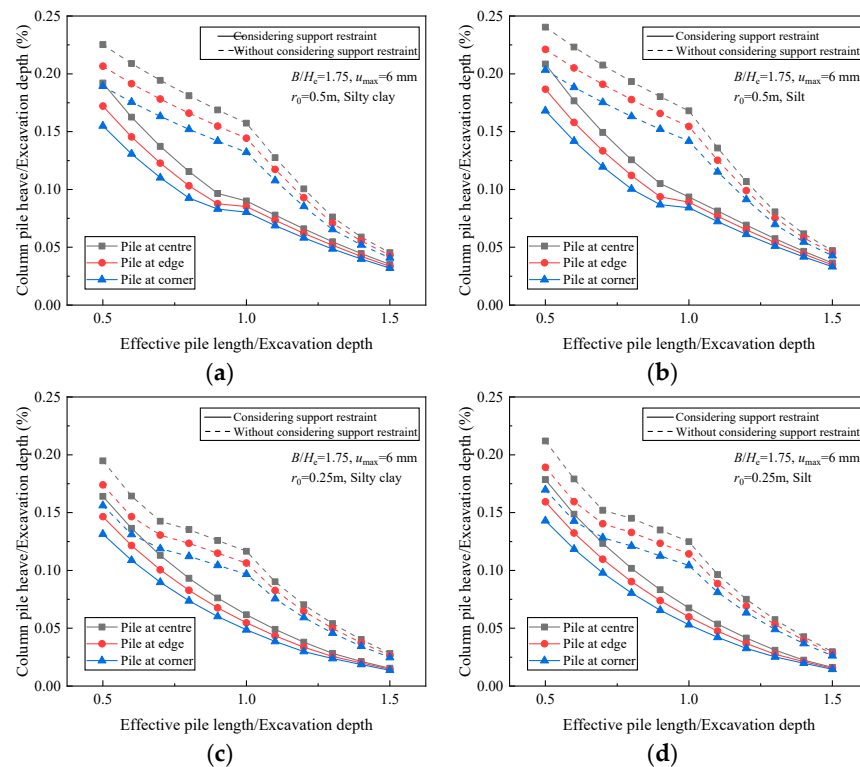


Figure 13. Effects of effective pile length on column pile heave with various positions of pile: (a) $r_0 = 0.5$ m with silty clay; (b) $r_0 = 0.5$ m with silt; (c) $r_0 = 0.25$ m with silty clay; (d) $r_0 = 0.25$ m with silt.

4.2. Effects of Excavation Width B

Figure 14 shows the relationship between column pile heave and excavation width B . It can be seen in this figure that the column pile heave increases with excavation width increase. In the case of considering the support restraint, the position of the pile has little influence on the results of column pile heave. The difference in column pile heave between the corner pile and the center pile will not exceed 10%. However, this factor cannot be ignored when the support constraint is not considered, especially in large excavations. Therefore, dividing the foundation pit into small blocks for excavation is a feasible method to reduce column pile heave.

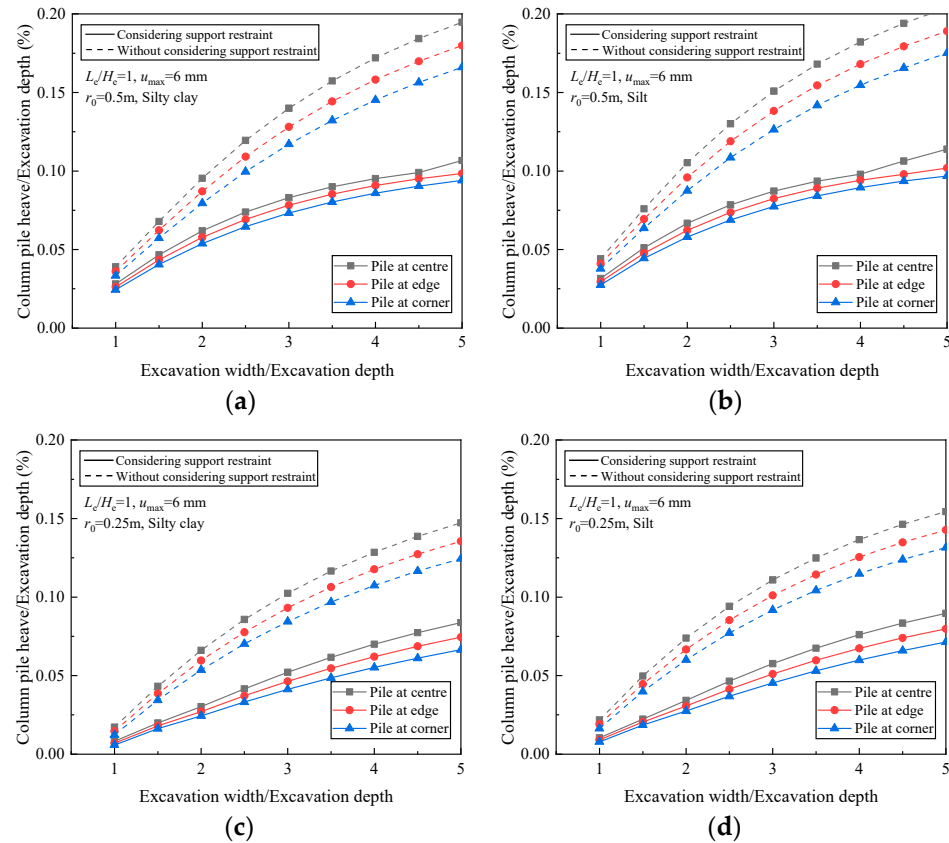


Figure 14. Effects of excavation width on column pile heave with various positions of pile: (a) $r_0 = 0.5$ m with silty clay; (b) $r_0 = 0.5$ m with silt; (c) $r_0 = 0.25$ m with silty clay; (d) $r_0 = 0.25$ m with silt.

4.3. Effects of the Limit Relative Displacement u_{max}

Figure 15 shows the relationship between column pile heave and limit relative displacement u_{max} . It can be seen in this figure that the column pile heave is hardly affected by the limit relative displacement in the range from 2 mm to 10 mm. There is a larger difference between the pile and the soil in modulus, which causes the pile-soil displacement to easily exceed the limit relative displacement when the soil rebound deformation occurs. Only the area near the neutral surface is within the limit relative displacement. Thus, the value of limit relative displacement can hardly affect the column pile heave. Similarly, the position of the pile has little influence on the results of column pile heave when the support constraint is considered but cannot be ignored when the support constraint is not considered. For small-diameter piles, ignoring the support constraint effect will seriously affect the column pile heave.

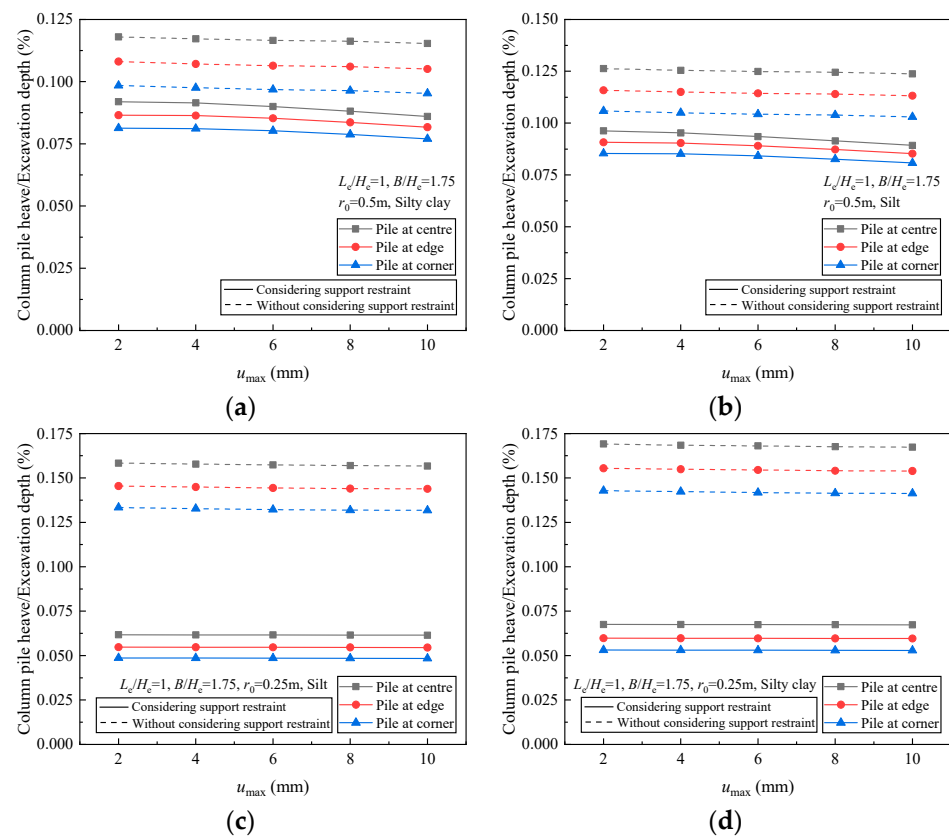


Figure 15. Effects of the limit relative displacement on column pile heave with various positions of the pile: (a) $r_0 = 0.5$ m with silty clay; (b) $r_0 = 0.5$ m with silt; (c) $r_0 = 0.25$ m with silty clay; (d) $r_0 = 0.25$ m with silt.

5. Conclusions

This paper proposed semi-analytical approach for calculating column pile heave during deep-foundation excavation, based on the RRM combined with the Mindlin stress solution. Compared to previous calculation methods, this method can consider the influence of soil disturbance by correcting soil parameters. The additional stresses in soil caused by the unloading and by the frictional resistance are obtained from the Mindlin stress solution, which enables the pile-soil load transfer and makes the calculation no longer limited to large-size excavations. In addition, support weight and restraint are taken in account. The calculation results obtained by the method proposed in this study after comprehensively considering these factors, which are significant in practical engineering, will be more in line with the actual situation. Based on the proposed approach, an effective iterative program was implemented. A parametric study was conducted to investigate the effect of excavation size and the limit of the relative displacement on column pile heave. The main conclusions can be summarized as follows:

1. The calculation method proposed in this paper reflects the development pattern of rebound deformation, and the results match measured values extremely well, validated by a field test. The method can also be used to calculate the development pattern of pile-side frictional resistance and pile axial force with excavation depth, providing theoretical basis and optimization guidance for the design of retaining structure and engineering piles below the bottom of the pit.
2. With increasing excavation depth, pile-soil interaction and column pile heave increase, leading to the redistribution of internal forces in the retaining structure and increasing the structural safety hazard. Tension will also be generated in the column pile. When the tension is too large, the pile will crack or break. For the CHIEF case study, the maximum pile tension was found to be 1100 kN; the measured and calculated ratios

of heave to excavation depth (S/H) were 0.0255% and 0.0248%, respectively. Therefore, enough attention should be paid to these problems in the engineering design and construction of deep excavation.

3. The excavation width B , the effective pile length L_e , and whether support restraints are considered will have a great impact on the results of column pile heave. The heave decreases more rapidly when the pile effective length is greater than the excavation depth. The support restraint causes a gentle stage in the heave versus the ratio of the pile effective length to the excavation depth curve in the range of 0.5–1.
4. When the excavation area is large or the effective pile length is short, the factor of the position of the column pile in the foundation pit cannot be ignored. The column pile heave is hardly affected by the value of the limit relative displacement.
5. The use of long piles with small diameter and the method of small block excavation are effective means to control the column pile heave.

Author Contributions: Conceptualization, K.Y. and Z.L.; methodology, K.Y.; validation, Y.C.; formal analysis, K.Y. and Z.L.; investigation, K.Y. and Y.C.; data curation, Y.C.; writing—original draft preparation, K.Y.; writing—review and editing, Z.L. and Y.C.; supervision, Z.L. and Y.C. All authors have read and agreed to the published version of the manuscript.

Funding: This research was funded by the foundations of the Center for Balance Architecture, Zhejiang University, and Key Laboratory of Soft Soils and Geoenvironmental Engineering (Zhejiang University), Ministry of Education, China (Grant: 2021P02).

Data Availability Statement: The raw data supporting the conclusions of this article will be made available by the authors on request.

Conflicts of Interest: The authors declare no conflict of interest.

Notation

The following symbols are used in this paper:

C_{LR}	Rebound index;
C_{FR}	Field recompression index;
$C_{FR,i}$	The field recompression index of the i -th layer of soil;
d	The pile diameter;
e_0	Initial void ratio;
e_{v0}	In situ initial void ratio;
$e_{v0,i}$	The in situ void ratio of the i -th layer of soil;
Δe_d	The decrease in the void ratio;
$E_{t,s}$	The unloading modulus of the i -th layer of soil;
f_s	The ultimate frictional resistance of the soil;
F_i	The weight of the i -th-layer horizontal support acting on the column;
h_i	The thickness of the i -th layer;
H_i	The thickness of the i -th layer of soil;
H	Excavation depth;
k_i	The restraint stiffness of the i -th-layer horizontal support to the column pile;
n_1	The total number of layers after discretization of the column pile;
n_2	The number of horizontal support layers;
p'_r	The residual effective stress;
Q	Force magnitude;
S	The final rebound displacement at the top of the column pile;
S_p	The pile top rebound displacement caused by the soil rebound deformation within the pile length;
S_s	The final soil rebound deformation;
S_{s1}	The rebound deformation of the soil below the pile end;
S_{s2}	The soil rebound within the range of pile length;
$S_{strut,i}$	The rebound deformation at the i -th-layer horizontal support;
u	The relative displacement between the soil and the pile;
u_{max}	The limit of the relative displacement;
z	The depth of calculation point;

σ_z	Bilinear distribution of concrete pressure;
σ'	The vertical effective stress on the side of the pile;
σ'_{v0}	The vertical effective stress before the excavation;
$\sigma'_{v0,i}$	The vertical effective stress of the i -th layer of soil before the excavation;
$\Delta\sigma_{z,i}$	The additional vertical effective stress of the i -th layer of soil;
$\Delta\sigma_{f,i}$	The additional stress caused by the frictional resistance of the pile in the i -th layer of soil;
μ	Poisson's ratio;
ρ	The horizontal distance between the calculation point and force;
ρ_i	The influence coefficient of a single vertically concentrated load in the i -th layer of soil;
τ	The pile-side frictional resistance;
τ_i	The frictional resistance around the column pile at the i -th-layer depth;
τ_j	The frictional resistance at the pile-soil interface of the j -th layer;
τ_{\max}	The ultimate value of the pile-side frictional resistance;
ξ	The pile-side frictional resistance coefficient.

References

- Zhu, H.-G.; Sun, J.-P. Impact of subsoil rebound on engineering piles due to deep excavation in soft soil area. *Geotech. Eng. World* **2005**, *8*, 43–46.
- Xu, Q.-G.; Xu, X.-H.; Liang, C.-H.; Jin, Y.-G.; Chen, N.-L. Influence of the deep excavation on the bottom piles. *Guangdong Archit. Civ. Eng.* **2006**, *1*, 33–34. [[CrossRef](#)]
- Chen, X.-X. The discussion of pile risk for bottom soil resilience with deep foundation pit excavation. *Fujian Constr. Sci. Technol.* **2006**, *3*, 15–16. [[CrossRef](#)]
- Mao, J.; Xu, W.; Lu, P. Vertical displacement analysis of erect column in deep foundation pit. *Archit. Technol.* **2004**, *35*, 342. [[CrossRef](#)]
- Liu, T.; Liu, W.; Liu, G. Discussions on vertical displacement of stud piles in deep foundation pit. *China Civ. Eng. J.* **2007**, *40*, 387.
- Wang, L.; Zheng, G.; Ou, R.N. Differential uplift and settlement between inner column and diaphragm wall in top-down excavation. *J. Cent. South Univ.* **2015**, *22*, 3578–3590. [[CrossRef](#)]
- Feng, J.; Tan, Y.; Ma, K.; Zhang, J.; Pan, T.; Yao, S.; Song, J.; Li, Z. Stability classification and construction method analysis of subway stations in upper-soft and lower-hard strata. *Eng. Fail. Anal.* **2023**, *153*, 107550. [[CrossRef](#)]
- Yuan, B.; Sun, M.; Xiong, L.; Luo, Q.; Pradhan, S.P.; Li, H. Investigation of 3D deformation of transparent soil around a laterally loaded pile based on a hydraulic gradient model test. *J. Build. Eng.* **2020**, *28*, 101024. [[CrossRef](#)]
- Liu, G.B.; Jiang, R.J.; Ng, C.W.; Hong, Y. Deformation characteristics of a 38 m deep excavation in soft clay. *Can. Geotech. J.* **2011**, *48*, 1817–1828. [[CrossRef](#)]
- Tan, Y.; Li, M. Measured performance of a 26 m deep top-down excavation in downtown Shanghai. *Can. Geotech. J.* **2011**, *48*, 704–719. [[CrossRef](#)]
- Tan, Y.; Wang, D. Characteristics of a large-scale deep foundation pit excavated by the central-island technique in Shanghai soft clay. I: Bottom-up construction of the central cylindrical shaft. *J. Geotech. Geoenviron. Eng.* **2013**, *139*, 1875–1893. [[CrossRef](#)]
- Tan, Y.; Wang, D. Characteristics of a large-scale deep foundation pit excavated by the central-island technique in Shanghai soft clay. II: Top-down construction of the peripheral rectangular pit. *J. Geotech. Geoenviron. Eng.* **2013**, *139*, 1894–1910. [[CrossRef](#)]
- Goh, A.T.C. Assessment of basal stability for braced excavation systems using the finite element method. *Comput. Geotech.* **1990**, *10*, 325–338. [[CrossRef](#)]
- Goh, A.T.C. Estimating basal-Heave stability for braced excavations in soft clay. *J. Geotech. Geoenviron. Eng.* **1994**, *120*, 1430–1436. [[CrossRef](#)]
- Goh, A.T.C.; Kulhawy, F.; Wong, K. Reliability assessment of basal-heave stability for braced excavations in clay. *J. Geotech. Geoenviron. Eng.* **2008**, *134*, 145–153. [[CrossRef](#)]
- Lu, P.-Y.; Yu, J.-X.; Xiao, J. Three-dimensional properties of foundation pit resilience under unloading. *J. Tianjin Univ.* **2006**, *39*, 301–305. [[CrossRef](#)]
- Yuan, B.; Li, Z.; Chen, W.; Luo, Q.; Yang, G.; Wang, Y. Experimental study on lateral cyclic loading model of pile-soil system based on PIV technique and fractal theory. *Chin. J. Rock Mech. Eng.* **2023**, *42*, 466–482. [[CrossRef](#)]
- Zheng, G.; Zhang, T.; Cheng, X.-S.; Diao, Y. Statistical analysis of measured data of center post upheaval in metro station excavations in Tianjin. *Rock Soil Mech.* **2017**, *38*, 387–394. [[CrossRef](#)]
- Yang, M.; Lu, J.-D. A calculation of behavior of underpinning pile subject to excavation of deep foundation pit. *J. Tongji Univ. Nat. Sci.* **2010**, *38*, 1730–1735. [[CrossRef](#)]
- He, C. Calculation of heave of soldier piles in deep foundation pits. *Chin. J. Geotech. Eng.* **2010**, *32* (Suppl. S1), 74–78. [[CrossRef](#)]
- Lou, X.-M.; Yang, J.; Li, D.-N.; Liu, J.-H. Uplift displacement of soldier piles during stepped excavation of deep foundation pits. *Chin. J. Geotech. Eng.* **2013**, *35*, 193–198. [[CrossRef](#)]
- Zhai, L.; Ding, Z.; Wang, J. Simplified calculation of heaving of soldier piles during excavation of foundation pits. *Chin. J. Geotech. Eng.* **2014**, *36* (Suppl. S2), 70–76. [[CrossRef](#)]

23. Ng, C.W. Observed performance of multipropped excavation in stiff clay. *J. Geotech. Geoenviron. Eng.* **1998**, *124*, 889–905. [[CrossRef](#)]
24. Lunne, T.; Berre, T.; Andersen, K.H.; Strandvik, S.; Sjursen, M. Effects of sample disturbance and consolidation procedures on measured shear strength of soft marine Norwegian clays. *Can. Geotech. J.* **2006**, *43*, 726–750. [[CrossRef](#)]
25. Zapata-Medina, D.G.; Finno, R.J.; Vega-Posada, C.A. Stress history and sampling disturbance effects on monotonic and cyclic responses of overconsolidated Bootlegger Cove clays. *Can. Geotech. J.* **2014**, *51*, 599–609. [[CrossRef](#)]
26. Li, Z.; Chen, Y.; Zhou, Y.; Bian, X. Field Rebound and Recompression Curve of Soft Clay. *Geotech. Test. J.* **2021**, *44*, 67–86. [[CrossRef](#)]
27. Mindlin, R.D. Force at a point in the interior of a semi-infinite solid. *Australas. Inst. Min. Metall. Publ. Ser.* **1936**, *7*, 195–202. [[CrossRef](#)]
28. Xu, L. Study on the Longitudinal Settlement of Shield Tunnel in Soft Soil. Ph.D. Thesis, Tongji University, Shanghai, China, 2005.
29. Tong, X.; Yuan, J.; Jiang, Y.-X.; Liu, X.-W.; Li, Y. Calculation of layered unloading additional stress of foundation pit based on Mindlin solution and the analysis of multiple factors influencing the rebound deformation. *Rock Soil Mech.* **2020**, *41*, 2432–2440. [[CrossRef](#)]
30. Liu, G.-B.; Huang, Y.-X.; Hou, X.-Y. A practical method for calculating a heave of excavated foundation. *China Civ. Eng. J.* **2000**, *33*, 61–67. [[CrossRef](#)]
31. Yu, J.-L.; Gong, X.-N. Research on deformation of foundation-pit engineering. *China Civ. Eng. J.* **2002**, *35*, 86–90. [[CrossRef](#)]
32. Richard, J.; Finno, M.J.; Tanner Blackburn, A.M.; Roboski, J.F. Three-dimensional effects for supported excavations in clay. *J. Geotech. Geoenviron. Eng.* **2007**, *133*, 30–36. [[CrossRef](#)]

Disclaimer/Publisher’s Note: The statements, opinions and data contained in all publications are solely those of the individual author(s) and contributor(s) and not of MDPI and/or the editor(s). MDPI and/or the editor(s) disclaim responsibility for any injury to people or property resulting from any ideas, methods, instructions or products referred to in the content.